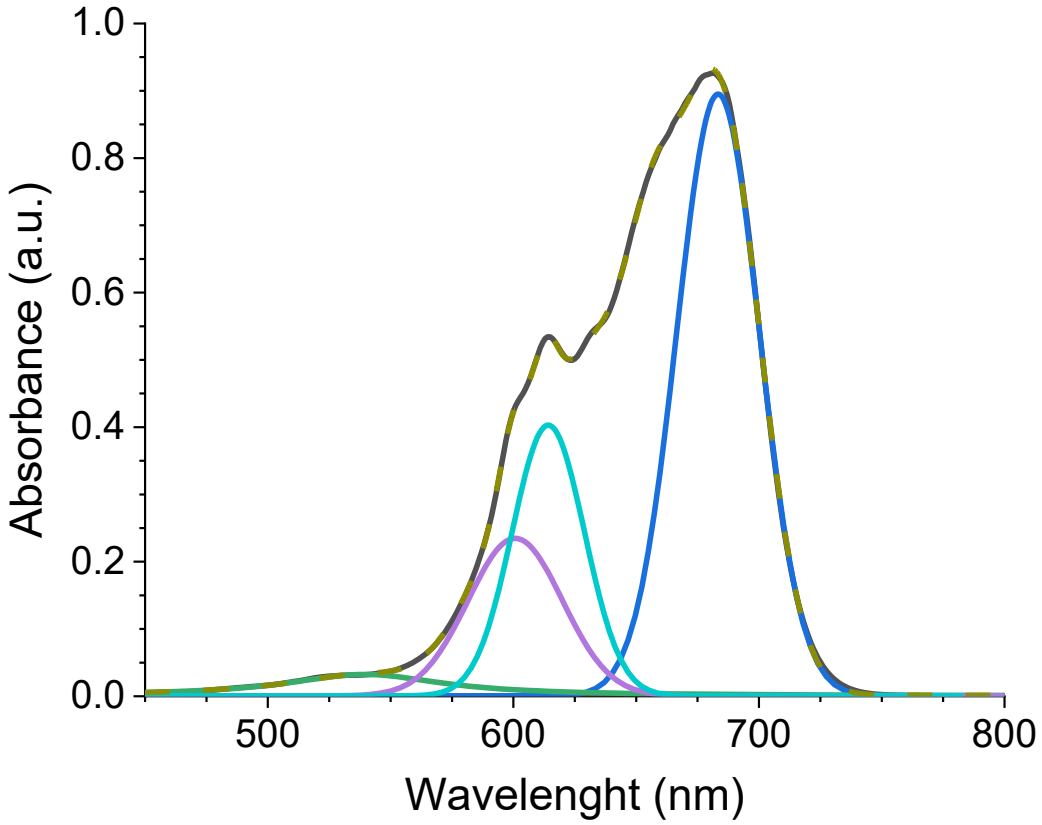



**Figure S1.** Band – resolved UV-Vis spectra of $CoCl_2$ in DMSO ($C_{CoCl2}$= 0.05 mol·l$^{-1}$) ($R^2$ = 99.6, $\chi^2$ = 7.23·10$^{-6}$).

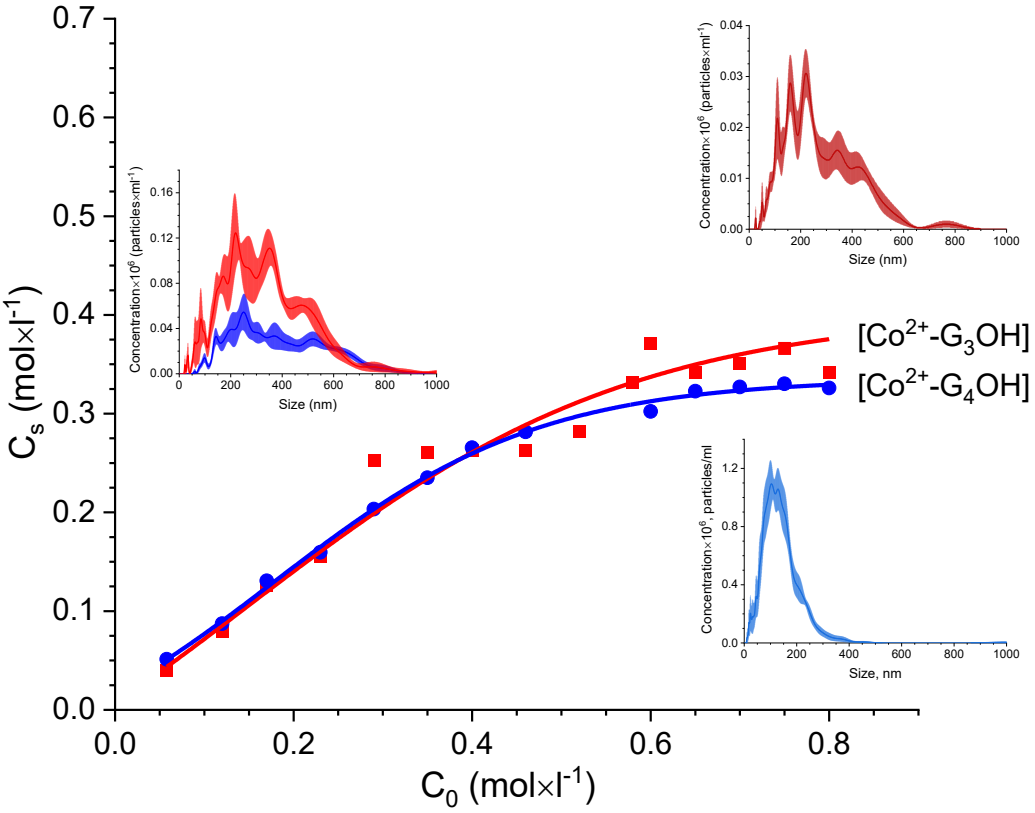



**Figure S2.** Distribution by size and number of particles in aqueous solution of $G_nOH$ [$Co^{2+}$ – $G_3OH$] and [$Co^{2+}$ – $G_4OH$], isotherms of sorption of $Co^{2+}$ ions by $G_3OH$ and $G_4OH$ matrix in DMSO solution ($C_{GnOH}$ = 0.125 g × ml$^{-1}$, $C_{Co2+}$ = 0.05-0.8 M).

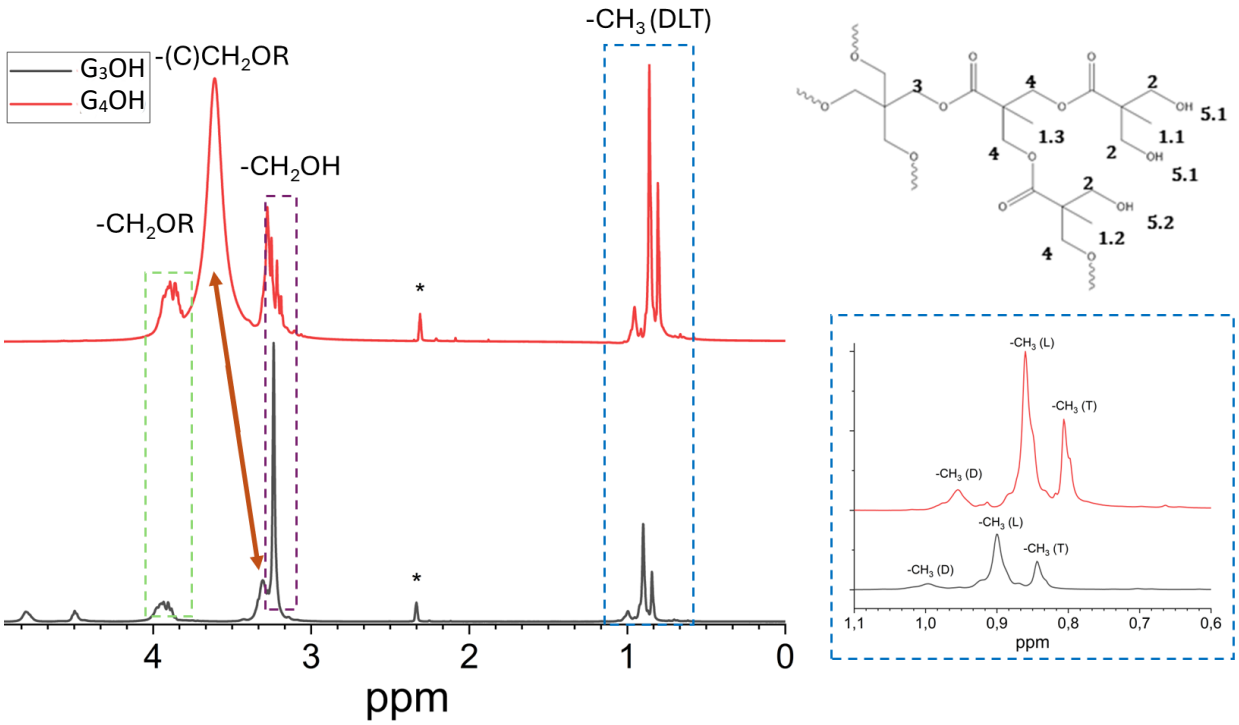



**Figure S3.** $^{1}$H NMR spectra of G$_3$OH and G$_4$OH in (CD$_3$)$_2$SO.

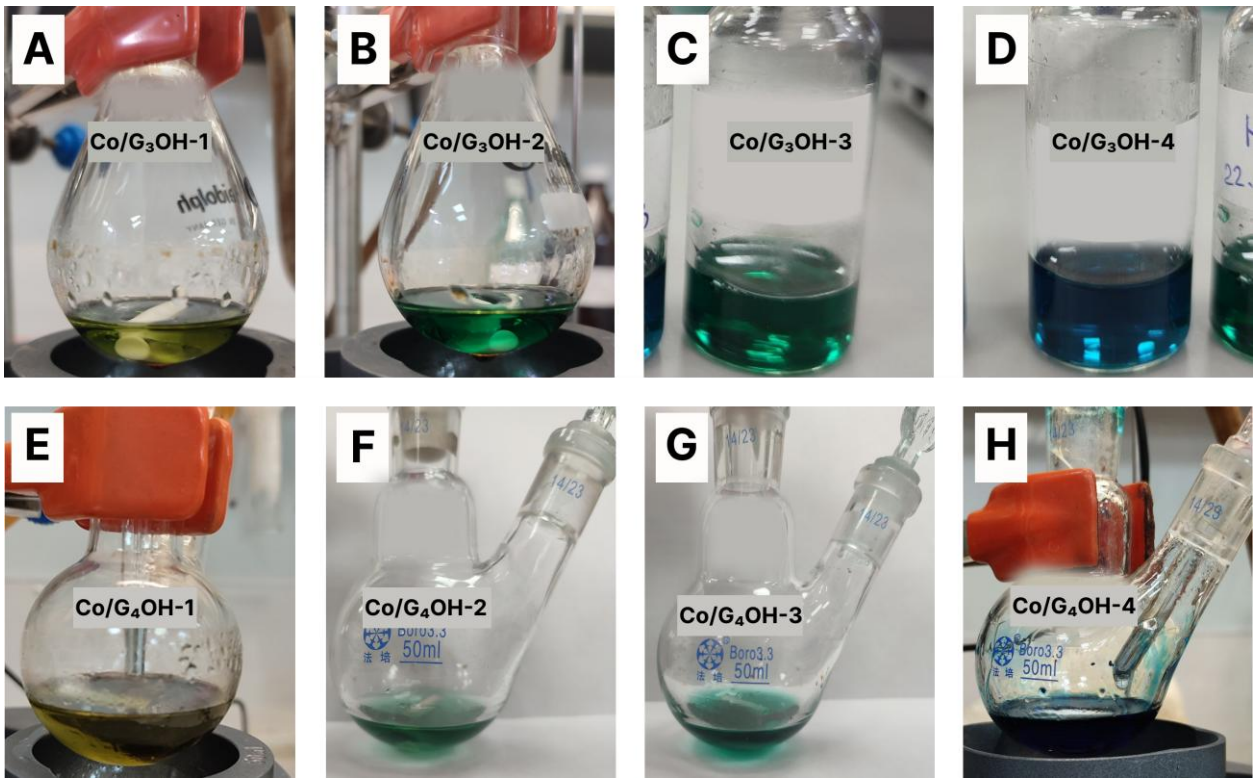



**Figure S4.** Appearance of the Co/GnOH reaction systems after completion of the synthesis: A-Co/G3OH-1, B- Co/G3OH-2, C- Co/G3OH-3, D - Co/G3OH-4, E- Co/G4OH-1, F- Co/G4OH-2, G- Co/G4OH-3, H- Co/G4OH-4.

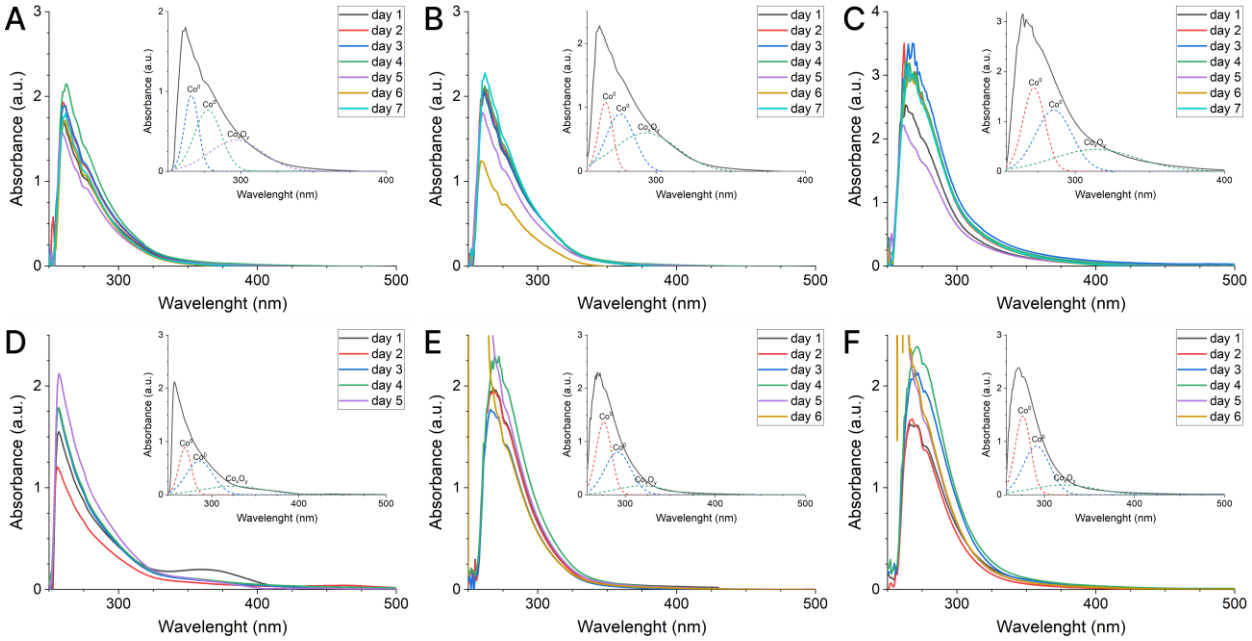



**Figure S5.** Evolution of electronic absorption spectra of dispersions of individual polymer-stabilized Co/G$_3$OH-1 (A) ($R^2$ = 99.6, $\chi^2 = 7.41 \cdot 10^{-5}$), Co/G$_3$OH-2 (B) ($R^2$ = 99.8, $\chi^2 = 5.41 \cdot 10^{-4}$), Co/G$_3$OH-3 (C) ($R^2$ = 99.7, $\chi^2 = 4.65 \cdot 10^{-5}$), Co/G$_4$OH-1 (D) ($R^2$ = 99.8, $\chi^2 = 5.42 \cdot 10^{-4}$), Co/G$_4$OH-2 (E) ($R^2$ = 99.7, $\chi^2 = 9.72 \cdot 10^{-4}$), Co/G$_4$OH-3 (F) ($R^2$ = 99.7, $\chi^2 = 1.37 \cdot 10^{-5}$) nanoparticles in water ($C_{Co/GnOH}$ = 2 mg/ml) and interpolation of absorption band from Gauss distribution function.

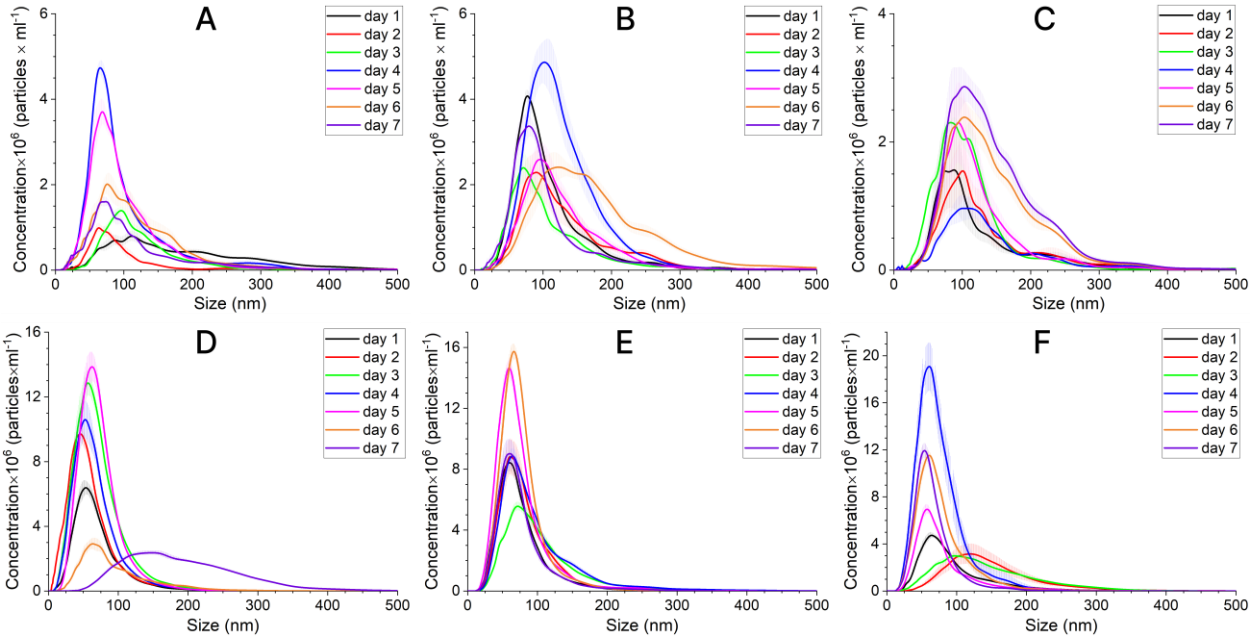



**Figure S6.** NTA Data of nanocomposite dispersions of Co/G3OH-1 (A), Co/G3OH-2 (B), Co/G3OH-3 (C), Co/G4OH-1 (D), Co/G4OH-2 (E), Co/G4OH-3 (F) ($C_{Co/GnOH}$ = 2 mg/ml) in the DMSO.

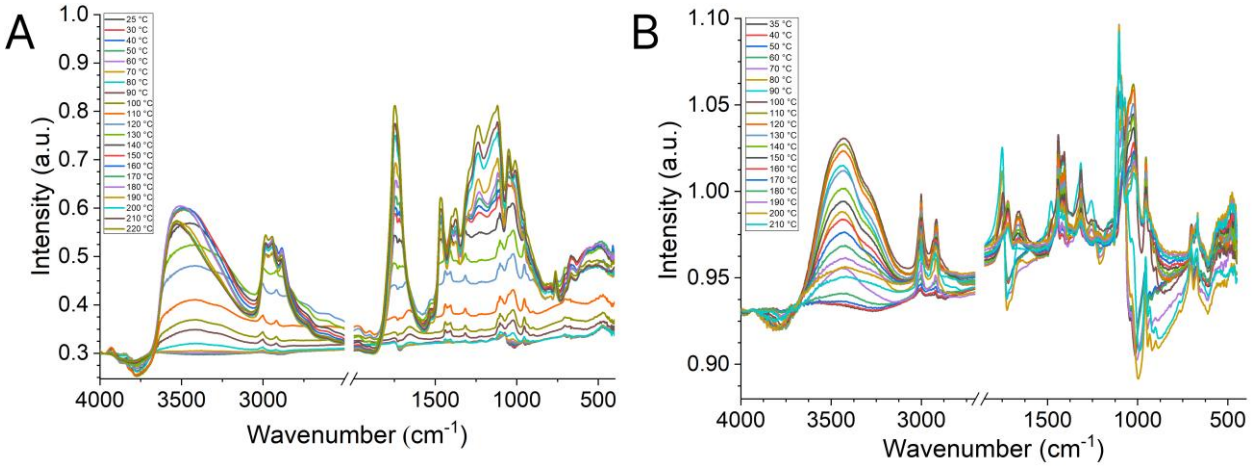



**Figure S7.** FT-IR spectra of diffuse reflectance of [$CoCl_2$-$G_3OH$] (A) and [$CoCl_2$-$G_4OH$] (B) mixture in situ when heated (T=35-210 °C, $C_{G3OH}$ = 0.629 g × $ml^{-1}$, $C_{Co2+}$ = 0.00258 g × $ml^{-1}$).

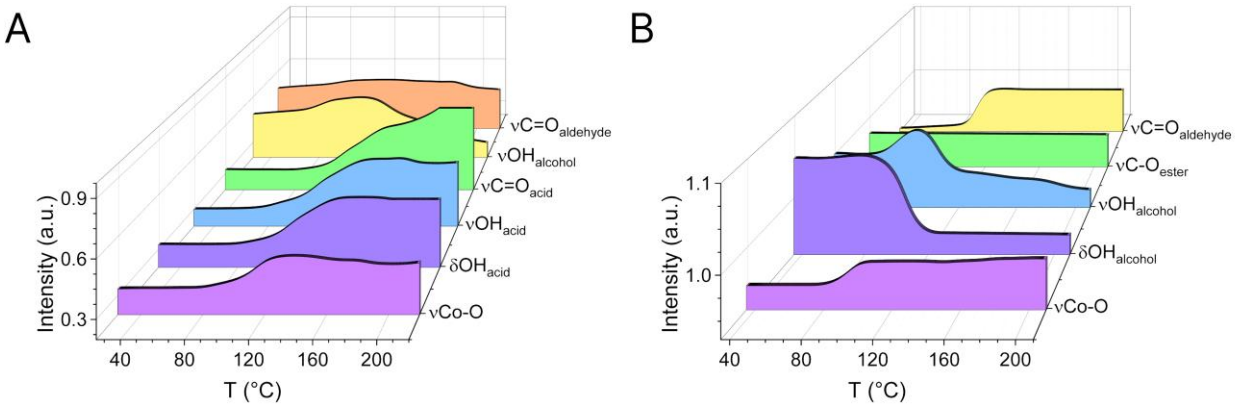



**Figure S8.** Profiles of intensity of characteristic bands in the IR diffuse reflectance spectra of the [$CoCl_2$-$G_3OH$] (A) and [$CoCl_2$-$G_4OH$] (B) mixture depending on the heating (T=35-210 °C, $C_{G4OH}$ = 0.629 g × $ml^{-1}$, $C_{Co2+}$ = 0.00258 g × $ml^{-1}$).

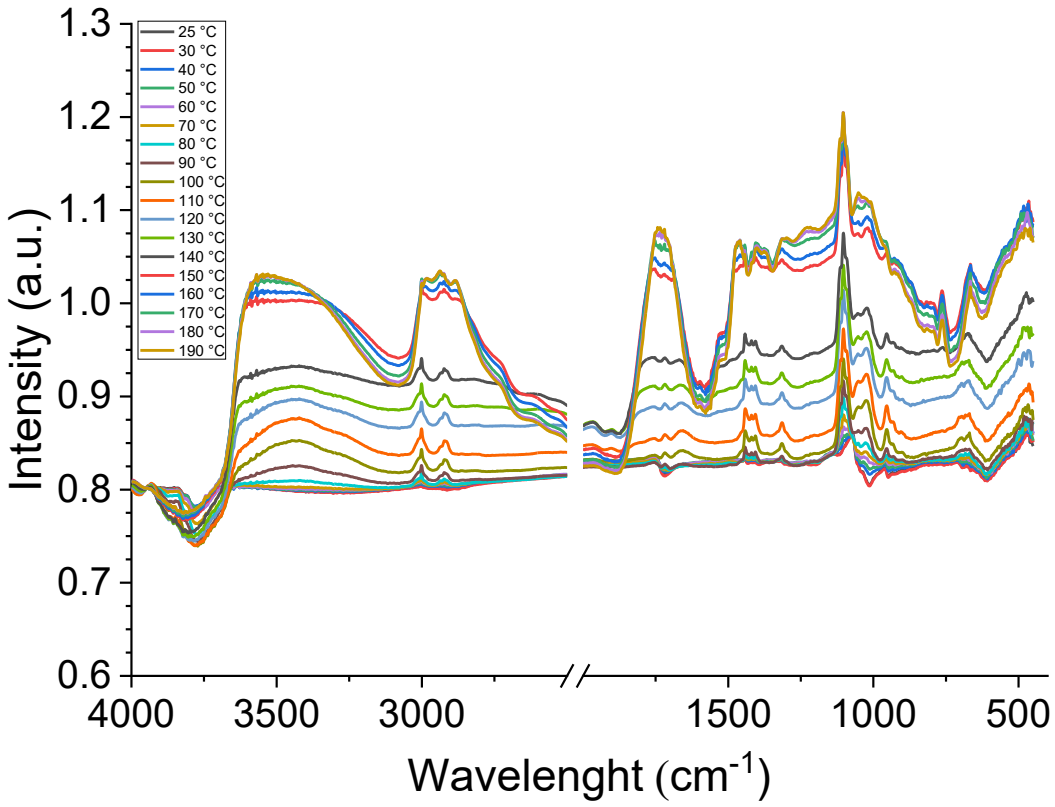



**Figure S9.** FT-IR spectra of diffuse reflectance of $G_4OH$ mixture *in situ* when heated (T=35-210 °C, $C_{G3OH}$ = 0.629 g × $ml^{-1}$).

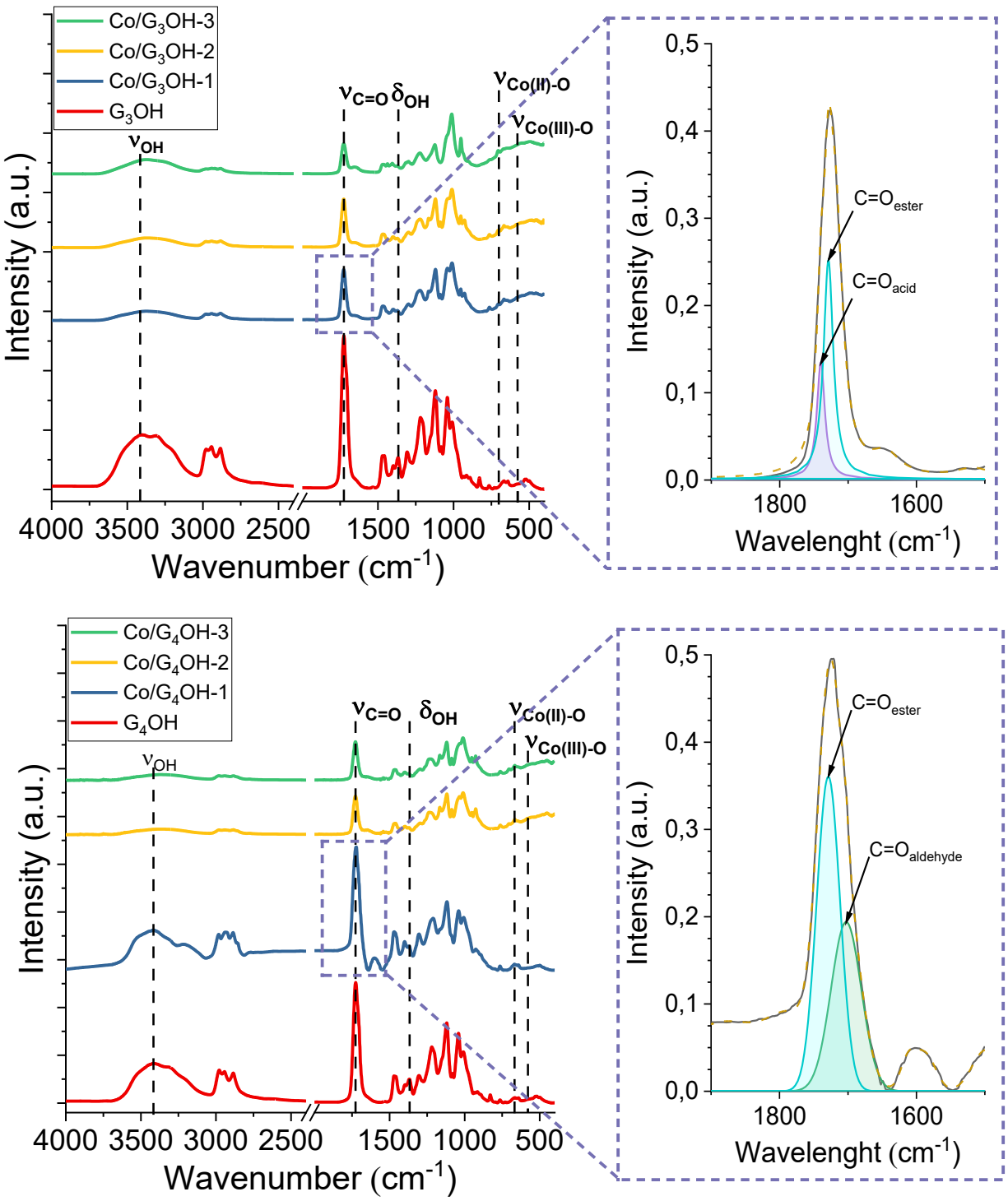



**Figure S10.** FT-IR spectra and the region of ester bonds with deconvolution for the initial and obtained compounds.

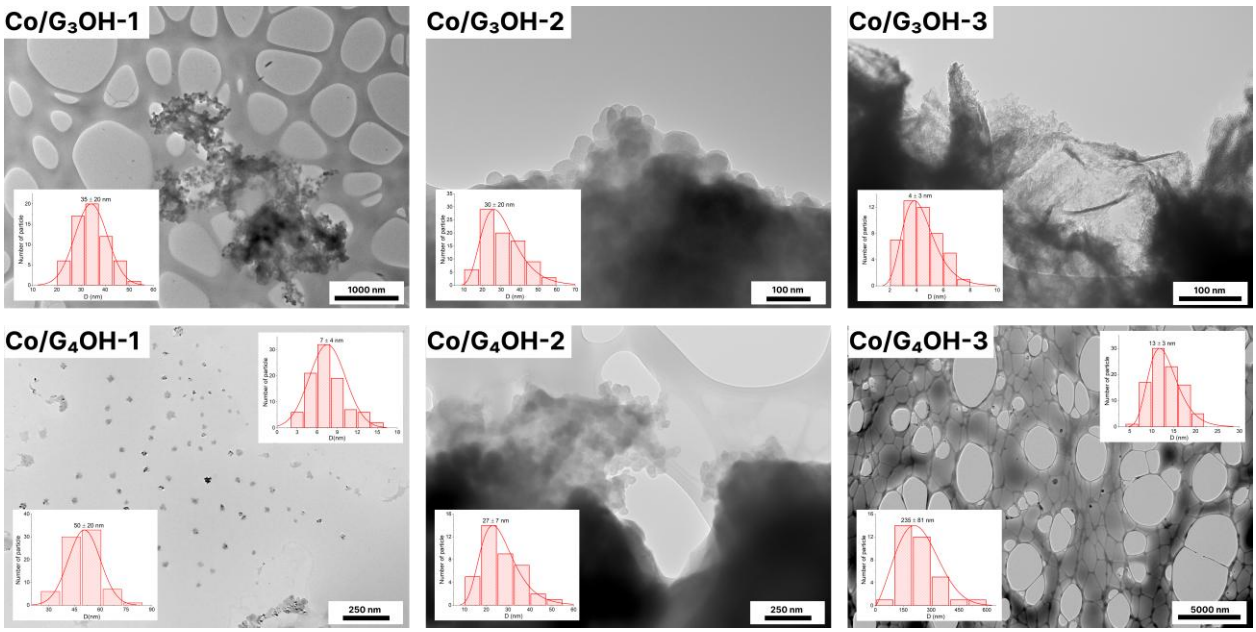



**Figure S11.** TEM images, particle size distribution and electron diffraction of Co/G3OH and Co/G4OH.

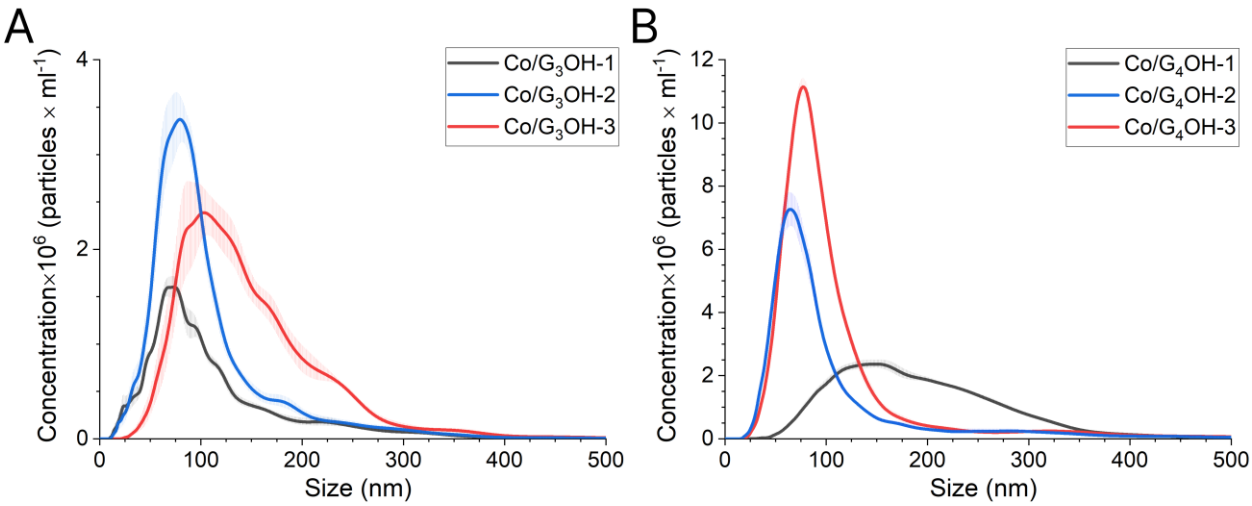



**Figure S12.** NTA data of nanocomposite dispersions Co/G3OH (A) and Co/G4OH (B) in the DMSO.

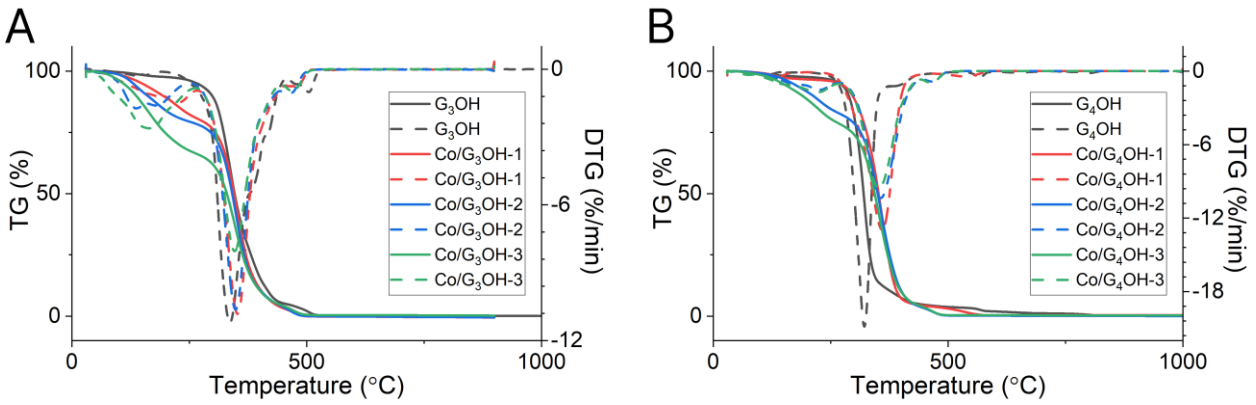



**Figure S13.** TG-DTG curves of Co/G3OH (A) and Co/G4OH (B) nanocomposites.

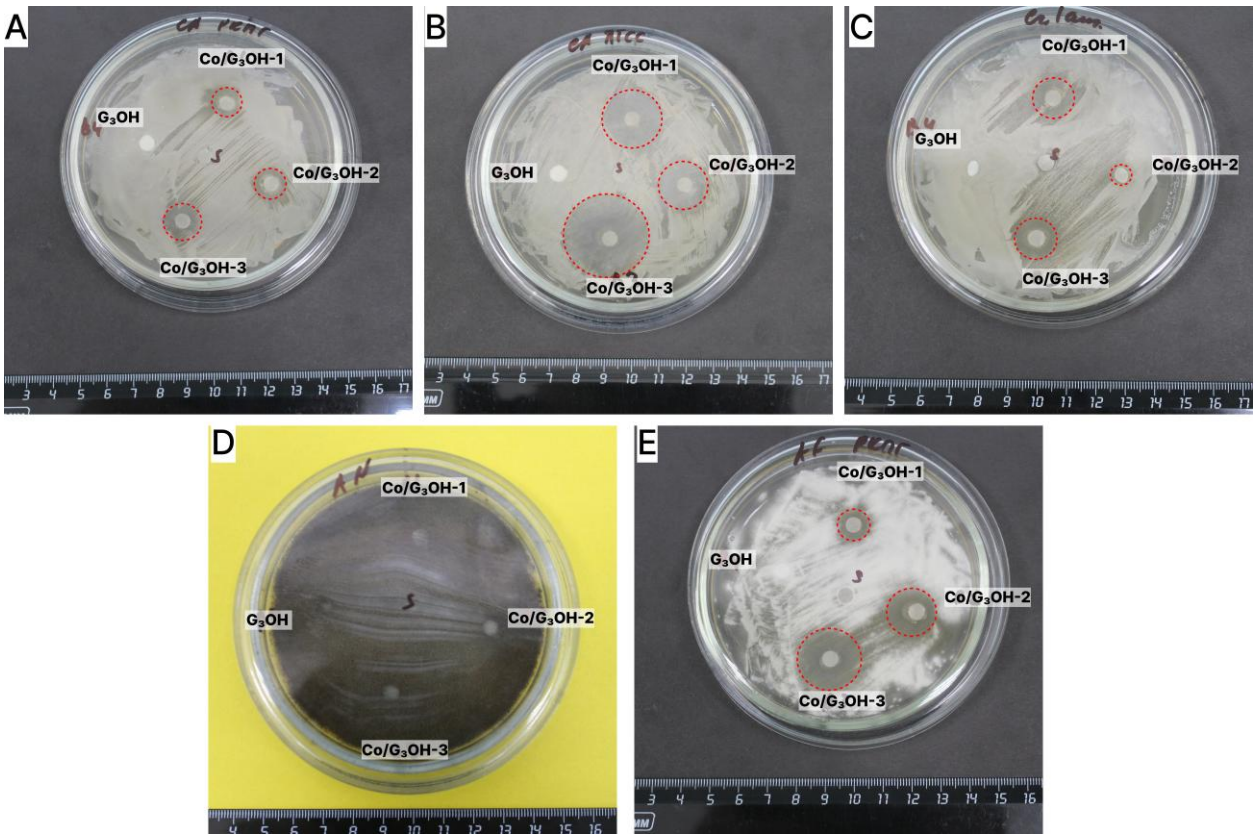



**Figure S14.** Zone of growth inhibition in assessing the sensitivity of *Candida albicans RCPF* (A), *Candida albicans ATCC 10201* (B), *Cryptococcus laurentii* (C), *Aspergillus niger F753* (D) and *Aspergillus fumigatus F1119* (F) to Co/G3OH.

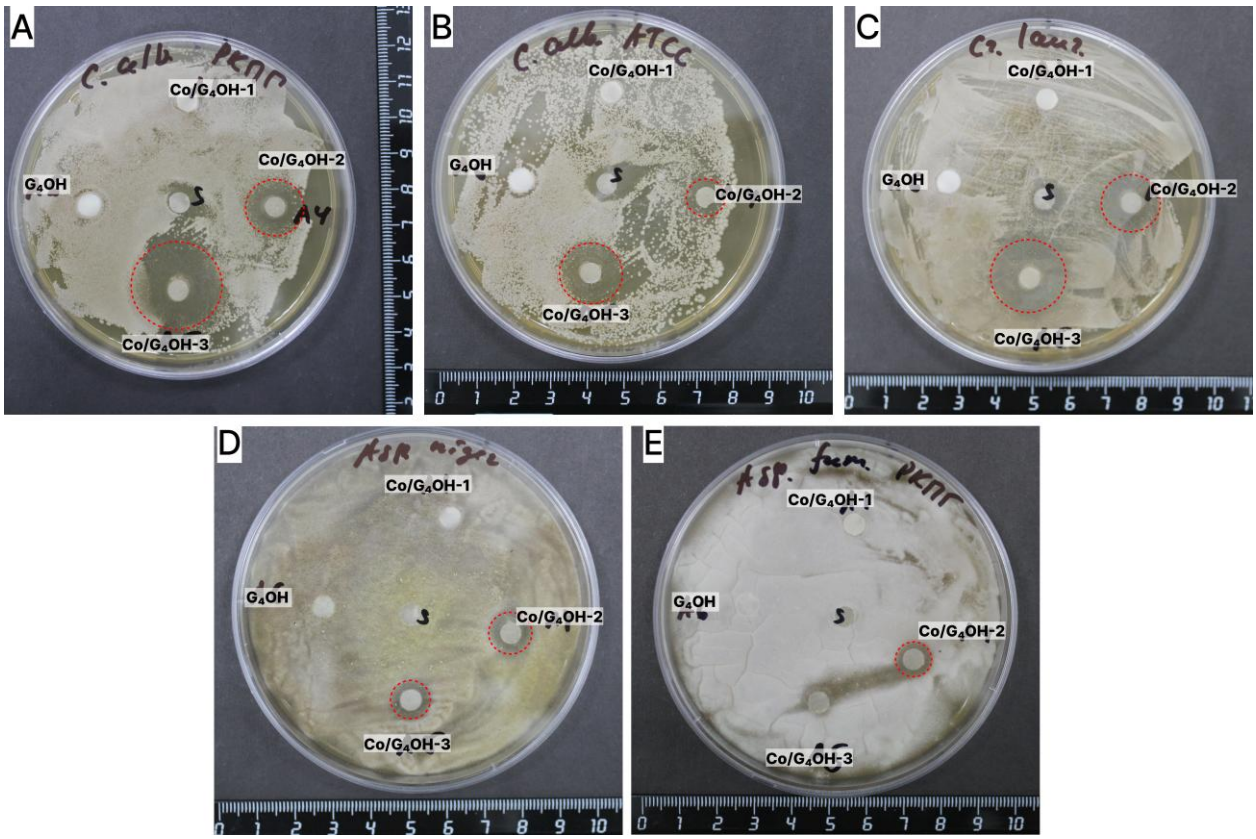



**Figure S15.** Zone of growth inhibition in assessing the sensitivity of *Candida albicans RCPF* (A), *Candida albicans ATCC 10201* (B), *Cryptococcus laurentii* (C), *Aspergillus niger F753* (D) and *Aspergillus fumigatus F1119* (F) to Co/G4OH.